

INL/CON-05-00528
PREPRINT

Modeling The GFR With RELAP5-3D

2005 RELAP5 International Users Seminar

C. B. Davis
T.D. Marshall
K. D. Weaver

September 2005

The INL is a
U.S. Department of Energy
National Laboratory
operated by
Battelle Energy Alliance



This is a preprint of a paper intended for publication in a journal or proceedings. Since changes may not be made before publication, this preprint should not be cited or reproduced without permission of the author. This document was prepared as an account of work sponsored by an agency of the United States Government. Neither the United States Government nor any agency thereof, or any of their employees, makes any warranty, expressed or implied, or assumes any legal liability or responsibility for any third party's use, or the results of such use, of any information, apparatus, product or process disclosed in this report, or represents that its use by such third party would not infringe privately owned rights. The views expressed in this paper are not necessarily those of the United States Government or the sponsoring agency.

MODELING THE GFR WITH RELAP5-3D

C. B. Davis, T. D. Marshall, and K. D. Weaver

Idaho National Laboratory
P. O. Box 1625
Idaho Falls, ID 83415-3890

ABSTRACT

Significant improvements have been made to the RELAP5-3D computer code for analysis of the Gas Fast Reactor (GFR). These improvements consisted of adding carbon dioxide as a working fluid, improving the turbine component, developing a compressor model, and adding the Gnielinski heat transfer correlation. The code improvements were validated, generally through comparisons with independent design calculations. A model of the power conversion unit of the GFR was developed. The model of the power conversion unit was coupled to a reactor model to develop a complete model of the GFR system. The RELAP5 model of the GFR was used to simulate two transients, one initiated by a reactor trip and the other initiated by a loss of load.

INTRODUCTION

The Department of Energy has chosen the Gas Fast Reactor (GFR) as chosen as one of six Generation IV systems to be evaluated based on its ability to meet the Generation IV goals in sustainability, economics, safety and reliability, and proliferation resistance and physical protection. The Idaho National Laboratory (INL) and the Massachusetts Institute of Technology (MIT) have been evaluating a version of the GFR that utilizes supercritical carbon dioxide in a direct Brayton cycle. The use of supercritical carbon dioxide allows the design to achieve a high thermal efficiency (~45%) with relatively modest reactor outlet temperatures (550 °C). Schematics of the GFR and the supercritical carbon dioxide cycle are shown in Figures 1 and 2.

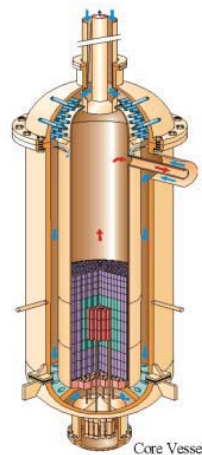


Figure 1. Schematic of the GFR.

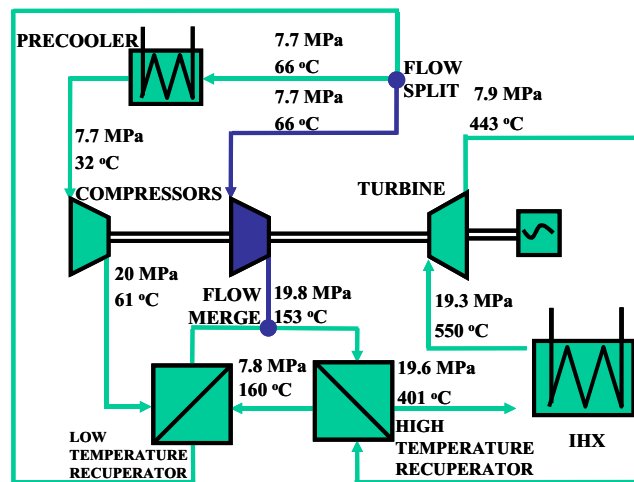


Figure 2. Schematic of the supercritical carbon dioxide cycle.

Significant improvements have been made to the RELAP5/ATHENA-3D (INEEL 2003a) computer code to support analysis of the GFR. These improvements include the addition of carbon dioxide as a working fluid in ATHENA, enhancements to the turbine model, development of a compressor model, and the addition of a forced convection heat transfer correlation that is believed to be more appropriate for the analysis of the GFR than the correlations previously included with the code.

The improved version of RELAP5/ATHENA was used to develop a model of the GFR power conversion unit (PCU). The model of the PCU was coupled to a model of the reactor vessel. The combined model was used to simulate two transients in the GFR, one initiated by a reactor trip and the other initiated by a loss of external load.

The remainder of this paper describes the code improvements made for the analysis of the GFR, the verification and validation activities that have been performed, the development of the GFR model, and the results of the transient analyses.

CODE IMPROVEMENTS

Carbon Dioxide Properties

Carbon dioxide properties were added to the RELAP5/ATHENA code to support analyses of the GFR. The thermodynamic properties were calculated with a detailed equation of state (McLinden et al. 1998 and Lemmon et al. 2002) developed by the National Institute of Standards and Technology (NIST). An interface was written to access the NIST database and write the thermodynamic properties in the format expected by ATHENA. The transport properties (thermal conductivity and viscosity) were also based the NIST database (Lemmon et al. 2002) and were implemented using tables. The implementation of thermodynamic and transport properties into ATHENA is described by Coryell and Davis (2002).

The implementation of the carbon dioxide thermodynamic properties was validated by comparing results of code-calculated values with an independent source of data (Perry 1950). The comparison concentrated on the subcritical gas and supercritical regions since these regions are of

primary interest for analysis of the GFR. Thermodynamic properties were compared for a wide range of pressures, from 0.8 to 20.7 MPa, and temperatures, from 227 to 1255 K. ATHENA calculations were performed at five specific pressure points and over the temperature range given by Perry. The comparisons between the values calculated by ATHENA and given by Perry are summarized in Figures 3 and 4, which show fluid density and specific enthalpy, respectively. A constant of 218.57 kJ/kg was subtracted from the enthalpy values reported by Perry to account for a different enthalpy datum. This value was obtained by subtracting the enthalpy predicted by the NIST database for saturated liquid at 0°C from the value used by Perry.

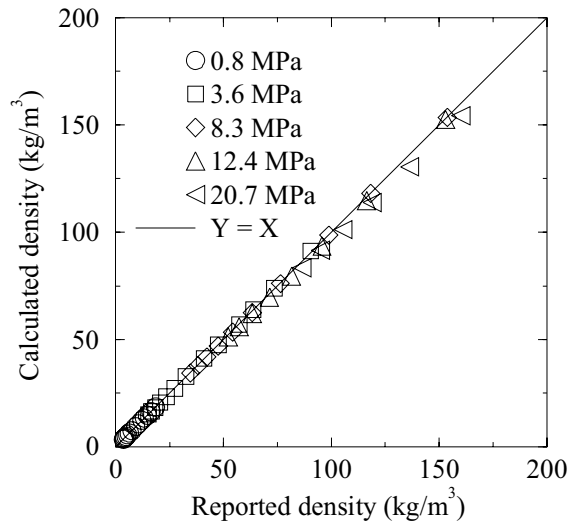


Figure 3. A comparison of calculated and reported fluid densities.

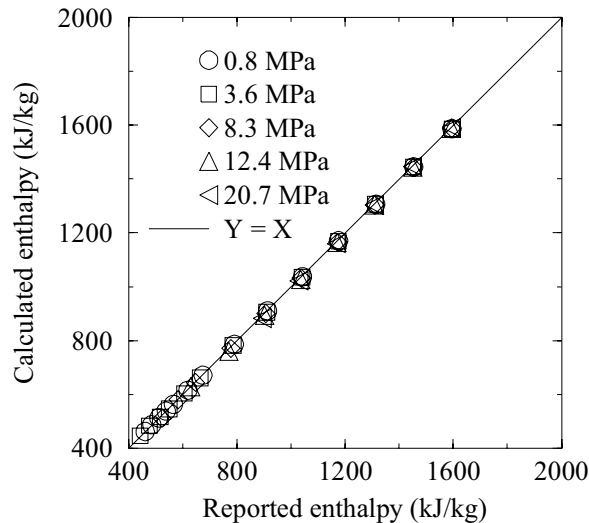


Figure 4. A comparison of calculated and reported specific enthalpies.

The fluid densities calculated by ATHENA were in excellent agreement with the values reported by Perry, as shown in Figure 3. On average, the densities calculated by ATHENA were within 1.0% of the values reported by Perry. The standard deviation, which was based on 51 data points,

was 1.3%. The largest deviation was 4.2% and occurred at the highest pressure. The difference between densities at 20.7 MPa, which was consistent as a function of temperature, was caused by differences between the NIST database and Perry. As expected, the results calculated by ATHENA were consistent with stand-alone calculations using the NIST database.

The specific enthalpies calculated by ATHENA were in excellent agreement with the values reported by Perry. On average, the enthalpies calculated by the code were within 0.4% of the values reported by Perry. The standard deviation was 0.5%. The largest deviation was 2.3%. For this case, the results calculated by ATHENA were also consistent with stand-alone calculations using the NIST database. Because the validation included variations in temperature at constant pressure, the agreement in specific heat capacity, which was not reported by Perry, is expected to be similar to that shown for enthalpy.

The specific enthalpy calculated by ATHENA was also compared with the values reported by MacDonald and Buongiorno (2001) for a supercritical Brayton cycle that is being considered for the secondary side of a fast reactor cooled by lead-bismuth. This Brayton cycle is very similar to the one planned for the GFR. Excellent agreement was obtained for this comparison. On average, the enthalpies calculated by ATHENA were within 0.2% of the values reported by MacDonald and Buongiorno. The standard deviation was 0.3%. The largest deviation was 0.8%. Good agreement was expected in this case because the values reported by MacDonald and Buongiorno were also generated with the NIST database, but the work was independent from that reported here.

The implementation of the transport properties was validated by comparison of ATHENA calculations with the data reported by Vesovic et al. (1990). The calculated and reported results were in excellent agreement, typically within 1%, as illustrated in Figures 5 and 6. The pressure and temperature ranges shown in Figures 5 and 6 encompass the expected operating region for the GFR.

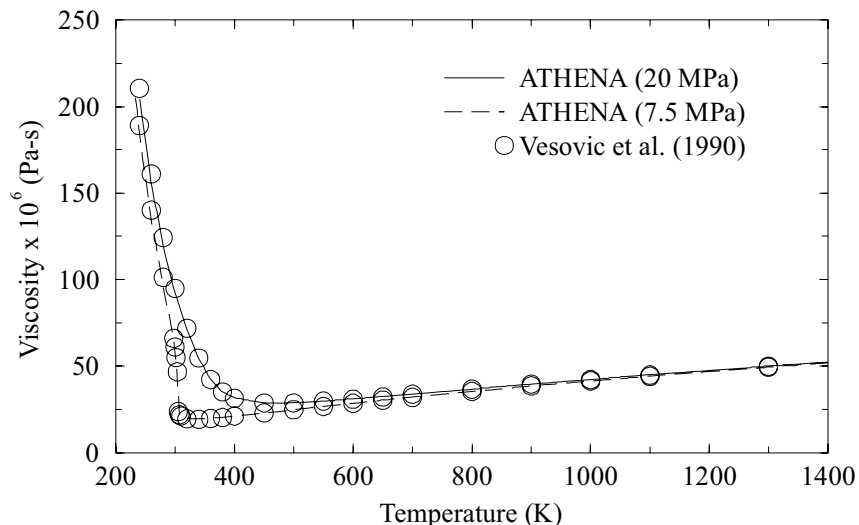


Figure 5. A comparison of calculated and reported values of dynamic viscosity.

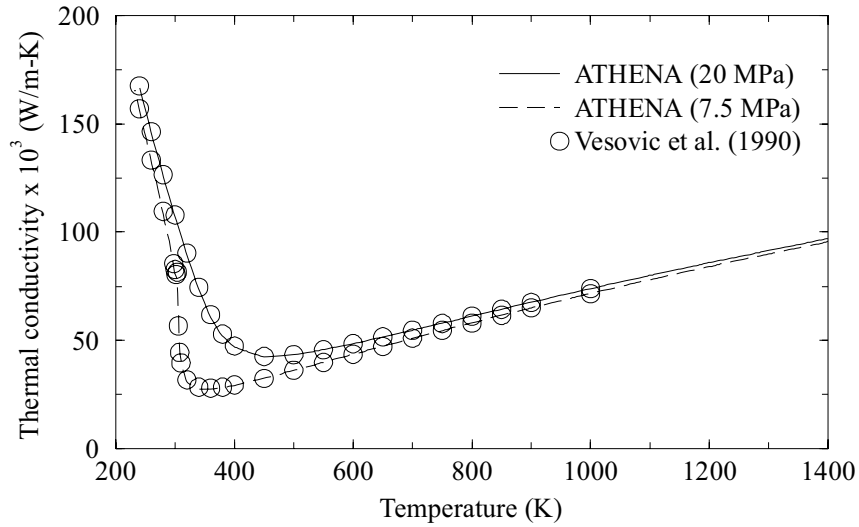


Figure 6. A comparison of calculated and reported values of thermal conductivity.

Turbine Model

The RELAP5-3D turbine model was evaluated for the turbine described by Dostal et al. (2002). The model in the original code was deficient because the power added to the shaft was not always consistent with the power removed from the fluid as shown in Figure 7. This deficiency was resolved by adding a dissipation term to the turbine energy equation. The shaft and hydraulic powers are now consistent for a wide range of flow rates. (The results shown in Figure 7 were obtained for exit Mach numbers between 0.25 and 0.70.) The flexibility of the turbine model was increased by allowing the user to account for variable frictional torque, variable moment of inertia, and adding a new type of turbine in which the user can specify the efficiency as a function of normalized speed and load.

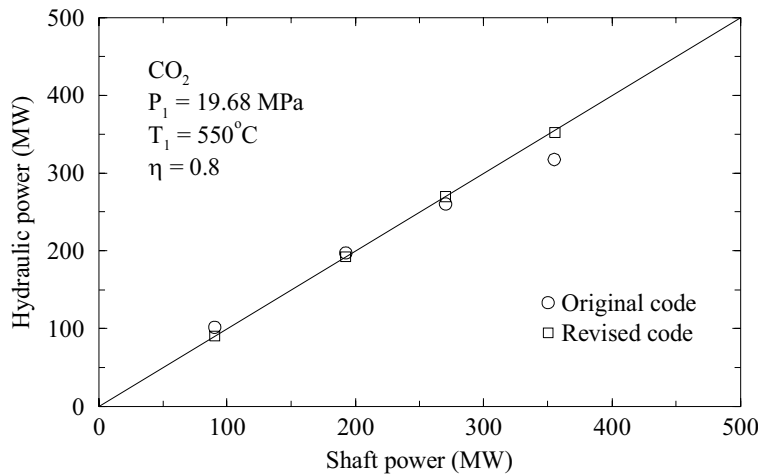


Figure 7. A comparison of hydraulic and shaft powers for a turbine.

The benchmarking of the improved turbine model against recent design calculations and its use during the transients are described later.

Compressor Model

A compressor component model was added to RELAP5/ATHENA for analysis of the GFR. The theory and implementation for the compressor model are described in detail by Fisher and Davis (2005). Compressor performance is characterized by tables of pressure ratio and efficiency as functions of relative corrected flow and relative corrected speed. These tables are obtained from design calculations or measurements. The compressor model was validated using design calculations from MIT. The results of these validations are described later.

Heat Transfer Correlation

The Gnielinski (1979) heat transfer correlation was added to RELAP5/ATHENA to support the analysis of the GFR. The Gnielinski correlation represents forced convection heat transfer for turbulent flow in pipes and channels. The code previously used the Dittus-Boelter (1930) correlation for forced convection heat transfer, but the Gnielinski correlation is now optionally available. The Gnielinski correlation simulates additional phenomena, including entrance effects, heated wall effects, and the transition between turbulent and laminar flow, compared to the Dittus-Boelter correlation. Furthermore, the Gnielinski correlation is applicable to both liquid and gas coolants. As described in INEEL (2003b), the heat transfer coefficient calculated by the code with Dittus-Boelter is 10% too high for helium at nearly adiabatic conditions.

SYSTEM MODEL DESCRIPTION

A RELAP5/ATHENA model of the GFR system was developed. The model represents the reactor vessel (see Figure 8), the passive Reactor Cavity Cooling System (RCCS) (see Figure 9) and the PCU (see Figure 10). Brief descriptions of the vessel and RCCS models are provided below. A detailed description of the PCU model is provided as this is a new application for RELAP5/ATHENA.

The model of the reactor vessel and core is based on the model developed by Marshall et al. (2005). The coolant enters and exits from the top of the reactor vessel through concentric ducts. The coolant flows down a downcomer (Component 140) and then upwards through the core (Components 160, 162, and 164). The core consists of prismatic blocks with uranium carbide fuel.

The RCCS model is based on one developed for the Next Generation Nuclear Plant (MacDonald et al. 2004). The RCCS is an air-cooled system. Atmospheric air enters the inlet plenum (Component 955) and then flows through the downcomer (Component 955), which is attached to the containment wall. The air then enters the bottom of the reactor compartment (Component 965), where it is distributed between many riser channels (Component 970), which are rectangular ducts. Heat is passively removed from the reactor vessel to the walls of the downcomer and the riser by a combination of radiation and natural convection. The heat is then transferred to the flowing air and rejected to the atmosphere.

The PCU model represents the supercritical carbon dioxide cycle developed by Dostal et al. (2004). The PCU contains a turbine (Component 315), a high temperature recuperator (Components 330 and 385), a low-temperature recuperator (Components 340 and 375), a

precooler (Components 360 and 610), a main compressor (Component 365), a recompressing compressor (Component 350), and various headers and plena. Components 305 and 395 represent the hot and cold legs of the cross vessel, respectively. Component 399 is a time-dependent volume that is used to control system pressure during steady-state calculations. During transients, Valve 398 is closed to isolate the system from the time-dependent volume.

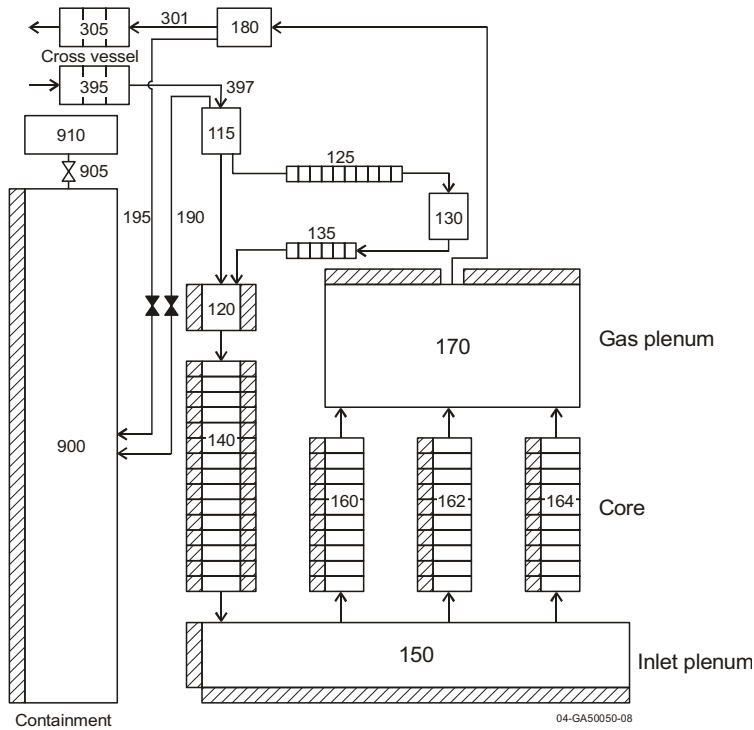


Figure 8. ATHENA model of the GFR reactor vessel.

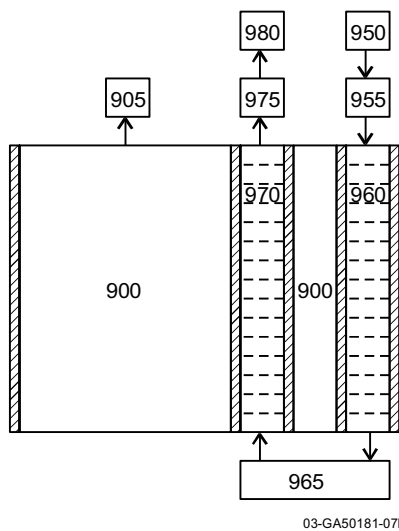


Figure 9. ATHENA model of the RCCS.

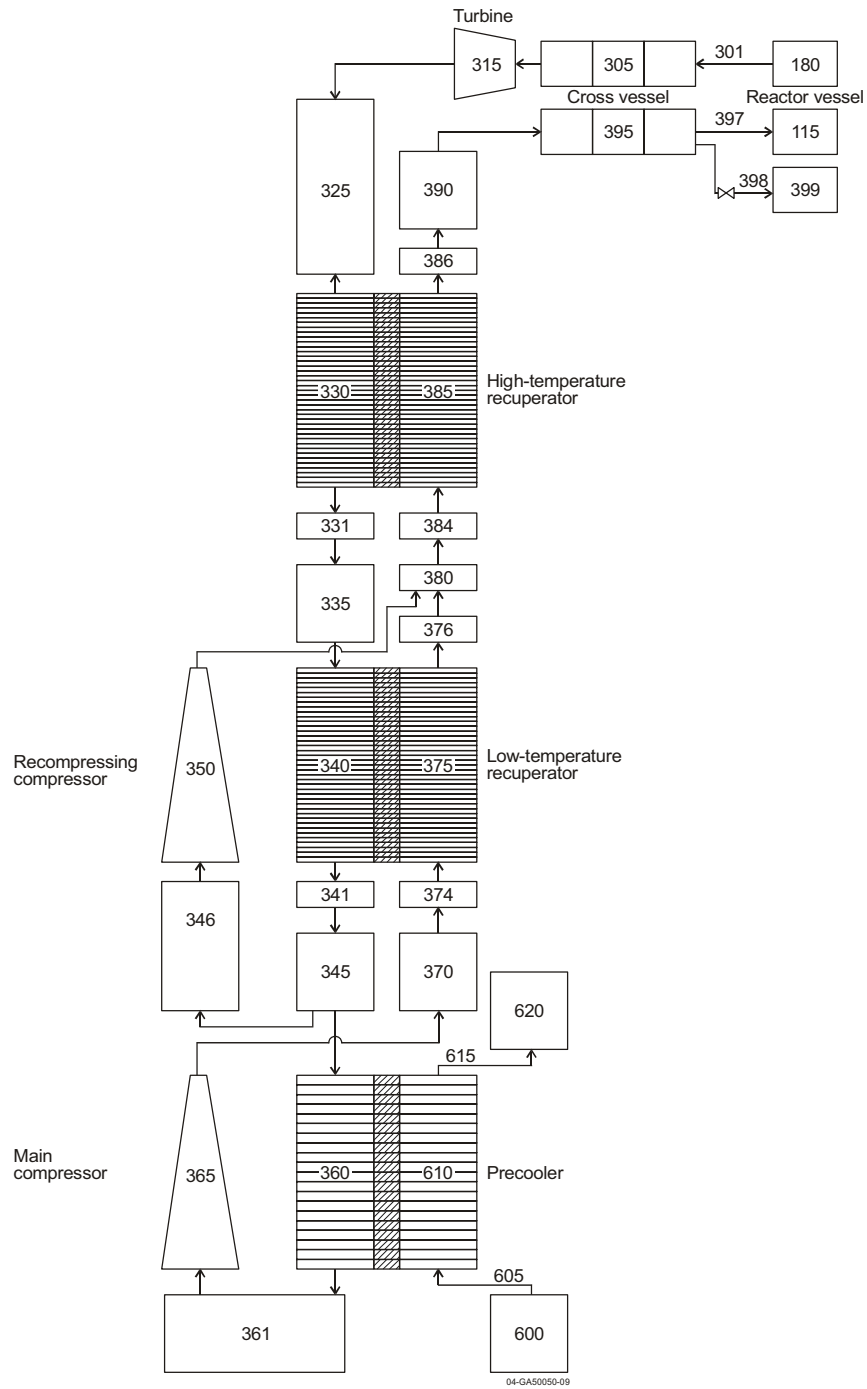


Figure 10. ATHENA model of the PCU.

Separate-effects models of the turbine, the three heat exchangers, and the two compressors were developed. Each separate-effects model represented the component of interest and adjacent control volumes. Boundary conditions were applied using time-dependent volumes and time-dependent junctions. Each component model was then adjusted to match desired conditions, which correspond to 550°C at the inlet to the turbine and 42°C at the inlet to the main

compressor. The 42°C value was chosen by Dostal et al. (2004) to prevent numerical instabilities in the design calculations for the main compressor, which operates near the critical point. Although the final design proposed by Dostal et al. (2004) calls for a compressor inlet temperature of 32°C (see Figure 2), performance curves for the compressors and turbine were not available for the 32°C design when the ATHENA model was being developed. Consequently, the ATHENA model is based on the preliminary design that utilized the 42°C value.

The turbine model was based on design calculations performed at MIT using the method described by Wang (2003). The results were transmitted to INEEL by Hejzlar (2004a) and correspond to the turbine design for a main compressor inlet temperature of 42°C. The turbine efficiency, η , which is defined as the ratio of actual turbine work to the ideal work produced by an isentropic expansion from the inlet stagnation state to the outlet stagnation state, was fit with a cubic polynomial

$$\eta = \eta_R(0.9407 + 0.0858 L - 0.0061 L^2 - 0.0188 L^3) \quad (1)$$

where η_R is the rated efficiency (= 0.929) and L is the turbine power normalized to a rated value of 375.4 MW. The form loss coefficient at the inlet to the turbine was adjusted to obtain the rated power at normal operating conditions. The separate-effects turbine model was then run at constant inlet conditions of 19.4 MPa and 550° C for a range of outlet pressures. Comparisons of the MIT design calculations with calculations from the ATHENA separate-effects model for mass flow rate and outlet temperature as functions of outlet pressure are presented in Figures 11 and 12. The results calculated with ATHENA were in reasonable agreement with the design calculations from MIT.

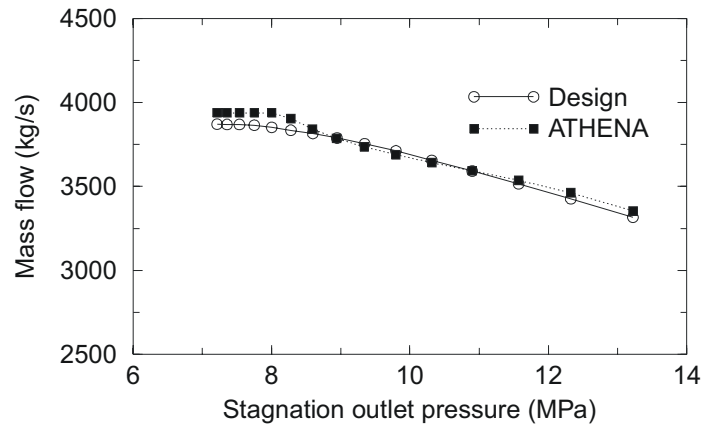


Figure 11. Mass flow rate through the turbine as a function of pressure.

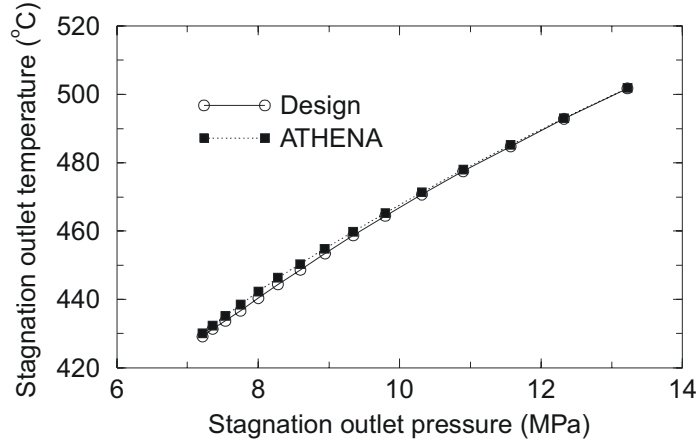


Figure 12. Fluid temperature at the outlet of the turbine as a function of pressure.

The main and recuperating compressor models were based on design calculations performed by Wang and transmitted to INEEL by Hejzlar (2004b). The models correspond to the designs for a main compressor inlet temperature of 42°C. The MIT design information was converted to the format expected by ATHENA. Specifically, the pressure ratio generated by the compressor and the efficiency were input as functions of relative corrected speed, α , and relative corrected flow, v , which are defined as

$$\alpha = \frac{N}{N_R} \frac{a_R}{a} \quad (2)$$

$$v = \frac{\dot{m}_R \rho_R a_R}{\dot{m}_R \rho a} \quad (3)$$

where N is the rotational velocity, a is the sonic velocity, \dot{m} is the mass flow rate, ρ is the fluid density, and the subscript R refers to a rated condition. The fluid density and sound speed are evaluated at stagnation conditions at the inlet to the compressor.

Figures 13 and 14 summarize the results of the MIT design calculations for the main compressor. Figure 13 presents the calculated stagnation pressure ratio for the main compressor versus the relative corrected flow for a range of relative corrected speeds varying between 0.10 and 1.0 while Figure 14 presents the calculated power consumed by the compressor at three different relative corrected speeds. The stagnation conditions at the inlet to the compressor were held fixed at the rated conditions of 9.07 MPa and 42°C during the design calculations. The figure also shows the surge and choke lines predicted by MIT. Compressor operation is allowed only within the relatively narrow band between the surge and choke lines. Pressure waves may be generated that might damage the compressor or other components if operation is attempted beyond the surge line.

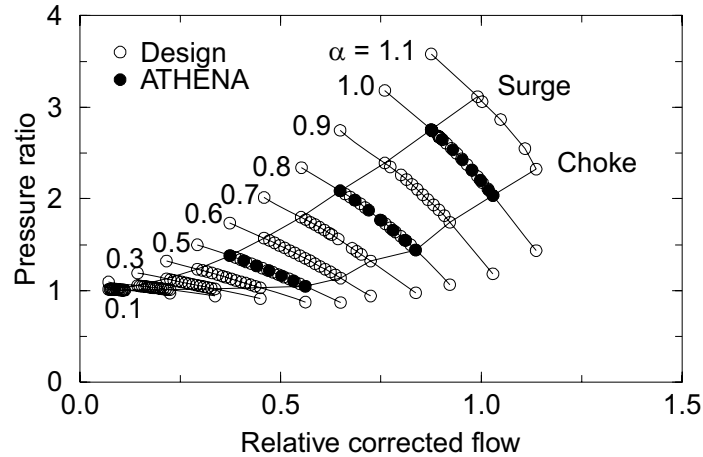


Figure 13. Pressure ratio developed by the main compressor.

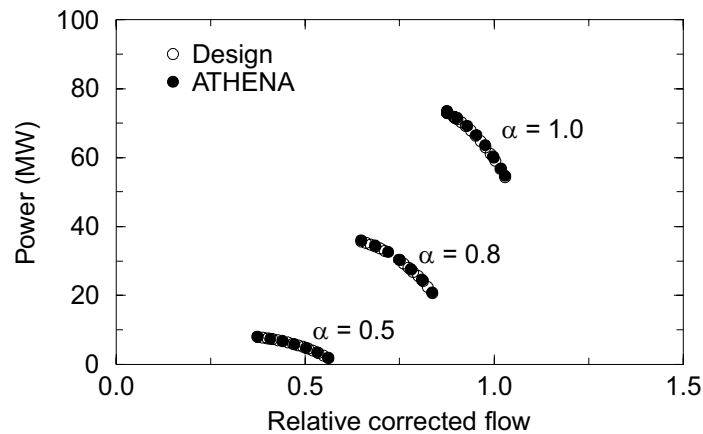


Figure 14. Power consumed by the main compressor.

The ATHENA compressor model requires that performance curves be available at relative corrected speeds and flows below and above the current operating condition so that an interpolation between adjacent curves can be performed. Consequently, the MIT results were extrapolated to a relative corrected speed of 1.1 to allow operation at the normal speed of 1.0. The performance curve at a given relative corrected speed was also extrapolated to the relative corrected flows corresponding to surge and/or choke lines of the adjacent speed curves so that the entire range of allowed operation could be simulated. The results of the calculations were monitored to determine if operation outside the surge and choke lines was attempted. The ATHENA separate-effects model of the main compressor simulated the allowed range of operation at three different relative speed curves, corresponding to values of 1.0, 0.8, and 0.5, in a series of steady-state calculations. As shown in Figures 13 and 14, the results calculated by ATHENA were in excellent agreement with the design calculations from MIT.

Figures 15 and 16 summarize the comparison between the MIT design calculations and the ATHENA separate-effects calculations for the recompressing compressor. The stagnation conditions at the inlet to the compressor were held fixed at the rated conditions of 9.08 MPa and 90°C during these calculations. ATHENA calculations were performed as a series of steady states at relative corrected speeds of 0.5, 0.8, and 1.0. As shown in the figures, the results

calculated by ATHENA were in excellent agreement with the design calculations from MIT for both the pressure ratio and the power consumed by the recompressing compressor.

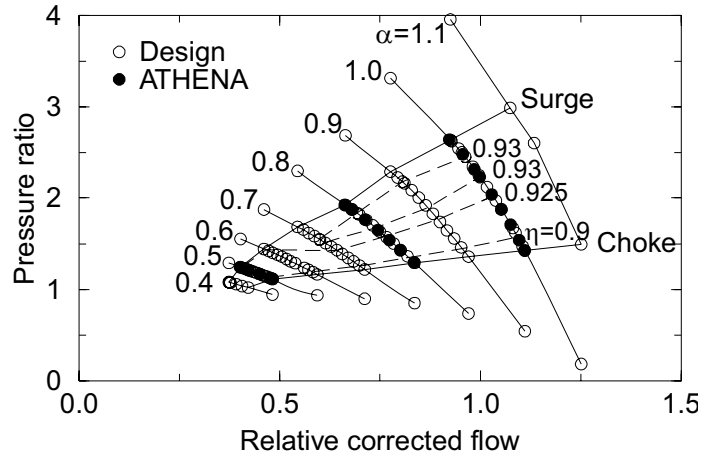


Figure 15. Pressure ratio developed by the recompressing compressor.

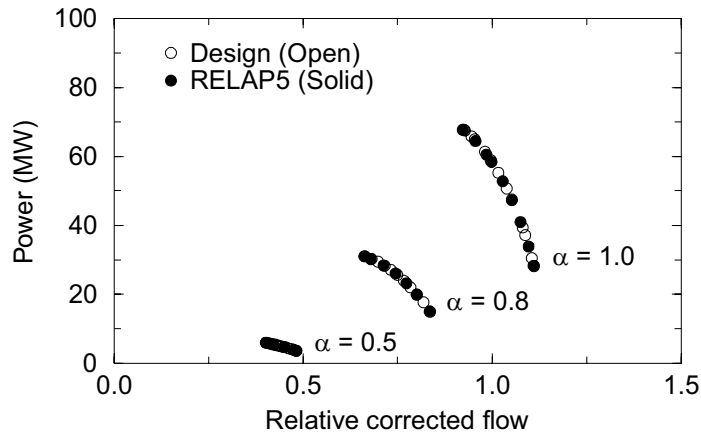


Figure 16. Power consumed by the recompressing compressor.

The PCU contains three heat exchangers, including the high-temperature and low-temperature recuperators and the pre-cooler. Each component is a printed circuit heat exchanger of the type manufactured by Heatric. These compact heat exchangers contain millions of small, semi-circular channels that are arranged in layers. Alternate layers contain hot and cold fluids that flow counter to each other. Supercritical carbon dioxide flows on both sides of the heat exchangers, except for the cold side of the pre-cooler which uses water.

The heat exchangers were optimized by MIT for the preliminary design with the 42°C inlet temperature at the main compressor. The resulting heat exchanger designs are summarized in Table 1. The ATHENA model was based on the information presented in the table. Because the details of the headers at the inlets and outlets of the heat exchangers were not available, form loss coefficients were adjusted to match the desired pressure drops given in Table 1.

Table 1. Heat exchanger designs.

Parameter	High-temperature recuperator	Low-temperature recuperator	Precooler
Active length, m	1.90	1.95	0.45
Semi-circular channel diameter, mm	2.00	2.00	2.00
Channel pitch, mm	2.40	2.40	2.40
Plate thickness, mm	1.50	1.50	1.50
Total number of channels	9,406,433	6,789,174	4,938,272
Hot side pressure drop, kPa	90.4	104.9	12.9
Cold side pressure drop, kPa	38.3	18.8	NA ¹
Total power, MW	986	413	345

1. Not available

The actual heat conduction between the hot and cold flow channels in these heat exchangers is multi-dimensional, but was approximated using one-dimensional heat conduction in a rectangular geometry. The thickness of the rectangular heat structure was assumed to be 0.9 mm, which corresponds to 60% of the plate thickness, based on the results of FLUENT calculations reported by Dostal et al. (2004). The heat transfer surface area in the model is the same as in the actual heat exchanger. The use of the geometrical surface area and an effective conduction thickness overestimates the volume of the heat structure by 14%. Consequently, the volumetric heat capacity of the metal was decreased by 14% to preserve the thermal capacitance of the heat structure. The Gnielinski (1976) heat transfer correlation was applied on both surfaces of the heat exchangers consistent with the analysis of Dostal et al. (2004). Relatively detailed nodalizations were used to obtain adequately converged solutions for the heat transfer across the counterflow heat exchangers. The high-temperature and low-temperature recuperators were modeled with 40 control volumes, while the precooler was modeled with 20 volumes. The separate-effects models of the high-temperature and low-temperature recuperators predicted total heat exchanger powers that were within 2% of the design values shown in Table 1. The heat transfer coefficients on both sides of the recuperators were increased using fouling factors to further improve the agreement in power. The water flow rate on the low-temperature side of the precooler was adjusted to match the power given in Table 1.

The separate-effects models of the turbine, compressors, and heat exchangers were then combined with the model of the reactor vessel shown in Figure 8 to form an integrated model of the primary coolant system. The models of the containment and the RCCS shown in Figure 9 were then added to form an integrated system model of the GFR. The system model was then used to generate a steady state. To improve the agreement with the design values, the form loss coefficient at the inlet to the turbine and the water flow rate through the precooler were adjusted by up to 10% from the values used in the separate-effects models.

Table 2 compares the design values from MIT with the results of the steady-state ATHENA calculation with the GFR system model. The results calculated by ATHENA are within a few percent of the design values. The fluid pressures and temperatures around the supercritical carbon dioxide cycle are shown graphically in Figure 17, where the arrows denote the direction of flow. The figure shows that the calculated results are in reasonable agreement with the desired values at all the points in the cycle. The maximum deviation in temperature between the design and calculated values was 7°C, and the results are within 2°C at the inlet and outlet of the reactor

vessel. Table 2 and Figure 17 show that the results of the steady-state ATHENA calculation are in reasonable agreement with the design values.

Table 2. A comparison of ATHENA calculated and design values for the GFR with a direct, supercritical carbon dioxide cycle.

Parameter	Design	ATHENA
Reactor power, MW	600	600
Reactor inlet temperature, °C	418.55	416.81
Reactor outlet temperature, °C	550.00	548.87
Main compressor inlet temperature, °C	42.00	42.23
Reactor inlet pressure, MPa	19.94	19.96
Mass flow rate, kg/s	3705.3	3654.8
Recompressed flow fraction	0.3042	0.3167
Precooler power, MW	345	333
Precooler water inlet temperature, °C	NA ¹	30
Precooler water flow rate, kg/s	NA ¹	8000
Maximum fuel temperature, °C	NA ¹	928
Shaft speed, rpm	3600	3600
RCCS heat removal, MW	NA ¹	1.1

1. Not available

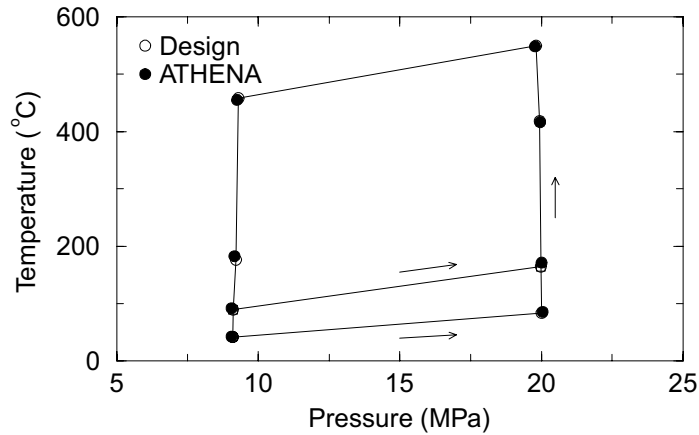


Figure 17. Pressure-temperature diagram for the supercritical carbon dioxide cycle.

A point kinetics model was implemented into the model to calculate reactivity effects due to various feedback mechanisms, including coolant density, Doppler, and core expansion. The coolant density coefficient was set to -0.00165 kg/m^3 , which corresponds to a 0.22% reactivity insertion if the core is voided (Hejzlar 2004c). Representative values of the other feedback coefficients were used because detailed design calculations were not available. The values selected were $-2.2 \times 10^{-3} \text{ }^\circ\text{C}$ for the Doppler coefficient, $-1.8 \times 10^{-3} \text{ }^\circ\text{C}$ for the radial expansion coefficient, and $-2.3 \times 10^{-4} \text{ }^\circ\text{C}$ for the axial expansion coefficient.

RESULTS

The ATHENA system model described previously was used to simulate two transients in the GFR. The transients selected for analysis included a reactor trip and a loss of external load. A transient initiated by a loss of flow was also briefly considered. In most reactors, loss of power to the pumps initiates loss of flow. However, in the GFR, the compressors and turbine are connected to a single shaft. Even if the connection to the external power grid is lost, the turbine will continue to supply power for the compressors. Thus, a loss of flow transient was not judged to be probable and was not analyzed. The results of the reactor trip and loss of external load transients are presented below. In addition, a calculation investigating the sensitivity of the steady-state fuel temperature to the convective heat transfer correlation was performed.

Reactor Trip

A transient initiated by a reactor trip was simulated using the ATHENA model illustrated in Figures 8 through 10. The transient was initiated at 5.0 s by a reactor trip. The control rod worth and insertion time were based on representative values for a pressurized water reactor. No other control or protective systems were assumed to operate during the transient.

The overall behavior of the GFR following a reactor trip is illustrated in Figure 18, which shows reactor power, core heat flux, generator power, and turbine flow. Each parameter was normalized to unity by dividing by its initial value. The control rod insertion that began at 5 s caused the reactor power to decrease rapidly. The decay power exceeded the fission power after 9 s, indicating that the reactor was essentially shut down. Because of the large thermal capacitance of the fuel blocks, the heat flux from the core decreased much slower than the reactor power. The net power applied to the generator decreased only slightly during the period of the calculation. The shaft speed remained constant because the generator was assumed to remain coupled to the electrical grid. Consequently, the head developed by the compressors and the flow rate through the turbine remained nearly constant.

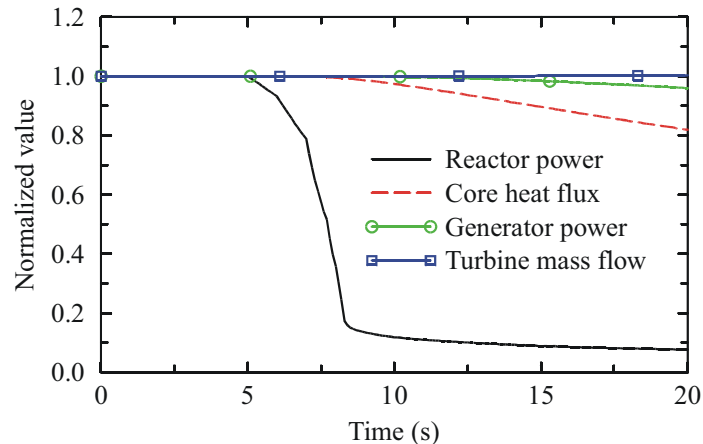


Figure 18. Normalized parameters following a reactor trip.

The thermal performance of the reactor is illustrated in Figure 19, which presents the fluid temperatures at the inlet and outlet of the reactor vessel as well as the maximum fuel temperature. The maximum fuel temperature decreased slowly following the reactor trip because of the large thermal capacitance of the fuel blocks. Although difficult to see because of the scale, the reactor

outlet fluid temperature also decreased slowly following the reactor trip. The slow decrease in the fluid temperature at the reactor outlet and the nearly constant flow rate through the turbine were responsible for the slow rate of decrease in the power supplied to the generator shown in Figure 18.

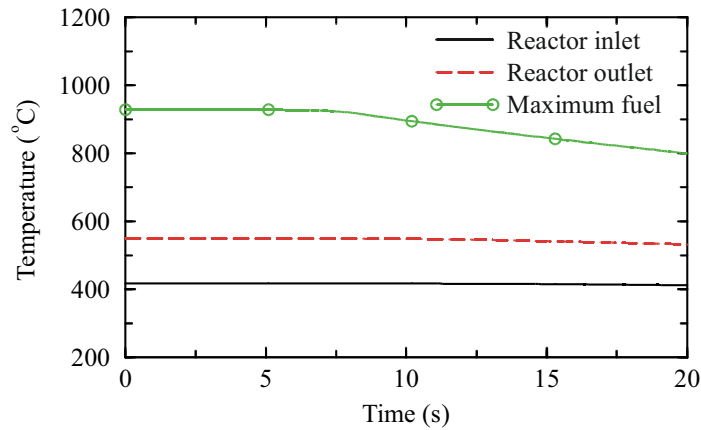


Figure 19. Reactor thermal response following a reactor trip.

The GFR responded slowly to the reactor trip. The compressors operated in the stable region between the surge and choke lines. Thus, the control system does not need to respond rapidly to protect the turbomachinery during this transient. The reactor will continue to supply power to the generator for a substantial period of time following the trip.

Loss of External Load

A transient initiated by a loss of external load decouples the generator from the external power grid. Because the shaft supplies power to the generator during normal operation, disconnecting the generator from the grid causes an imbalance in the shaft torque that causes it to accelerate. The response of the system to the loss of load will be strongly affected by the plant's control systems, which will attempt to control reactor power and protect the turbomachinery by bypassing flow from the turbine (Dostal et al. 2004). Because the control systems for the GFR have not been designed yet, this analysis was performed without any control systems to determine the natural response of the plant and to aid in determining the time available for the control systems to respond.

Preliminary calculations of the transient initiated by a loss of external load resulted in an increase in the shaft speed by more than a factor of two. The compressor design data originally supplied by MIT only investigated the effects of reductions, not increases, in shaft speed. Because of the major extrapolation required in the performance curves, it was decided that the extrapolated compressor behavior could be better simulated using a homologous form based on a centrifugal pump model. The MIT design data for the main compressor are shown in homologous form in Figures 20 and 21 for the main compressor. The independent variables in the homologous format are the speed, α , and flow, v , ratios, where

$$\alpha = \frac{N}{N_R} \tag{4}$$

$$v = \frac{Q}{Q_R} \quad (5)$$

and N is the shaft speed, Q is the volumetric flow rate, and the subscript R refers to the rated condition. The volumetric flow was computed from the mass flow rate and the average of the inlet and outlet fluid densities, $\bar{\rho}$. The dependent variables in the homologous format are the dimensionless head, h , and torque, β , which are calculated as

$$h = \frac{H}{H_R} \quad (6)$$

and

$$\beta = \frac{\tau}{\tau_R} \quad (7)$$

where

the head, H , and torque, τ , are calculated as

$$H = \frac{\Delta P}{\bar{\rho}g} \quad (8)$$

and

$$\tau = \frac{\bar{\rho}_R QgH}{N\eta} \quad (9)$$

where ΔP is the pressure rise developed by the compressor, g is the acceleration due to gravity, and η is the efficiency. A significant increase in the scatter of the homologous curves was obtained when the inlet or outlet fluid density was used in the calculation of the volumetric flow, pump head, and torque rather than the average density.

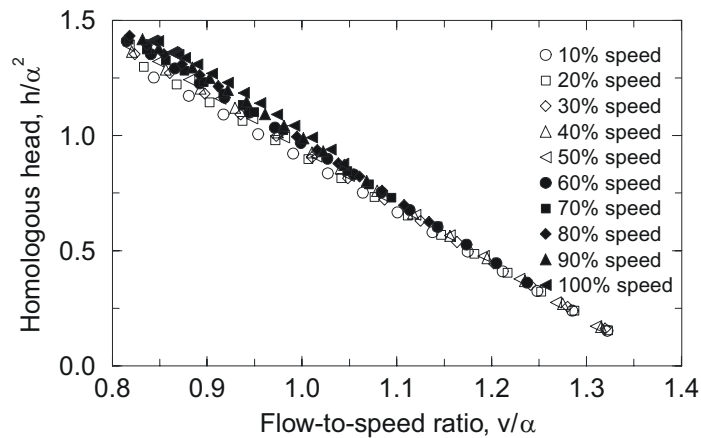


Figure 20. Homologous head for the main compressor.

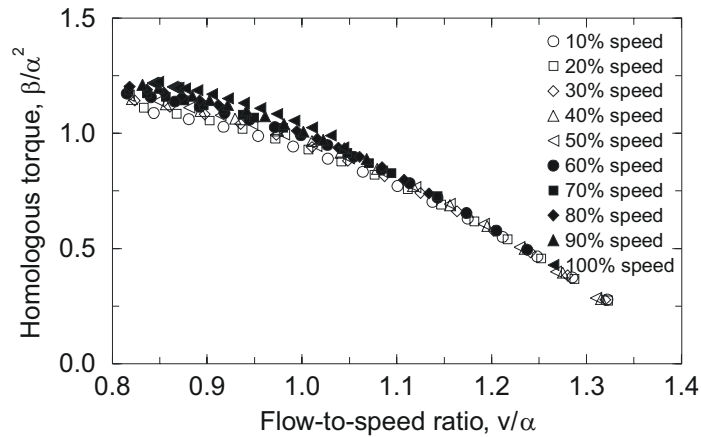


Figure 21. Homologous torque for the main compressor.

Figures 22 and 23 show homologous head and torque for the recompressing compressor. The scatter is generally less than that obtained for the main compressor, probably because the recompressing compressor operates farther away from the critical point. The scatter for the recompressing compressor was somewhat higher for the three data points with the highest flow rate for the case at 40% speed. This increased scatter was caused by the rear stages of the compressor acting as a turbine, and removing energy from, rather than imparting it to, the fluid.

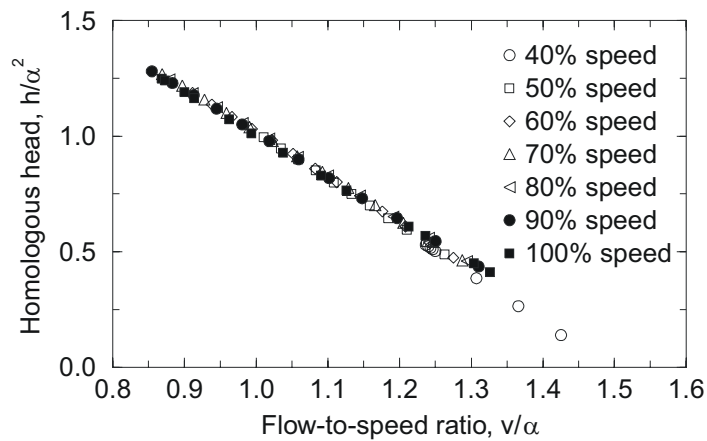


Figure 22. Homologous head for the recompressing compressor.

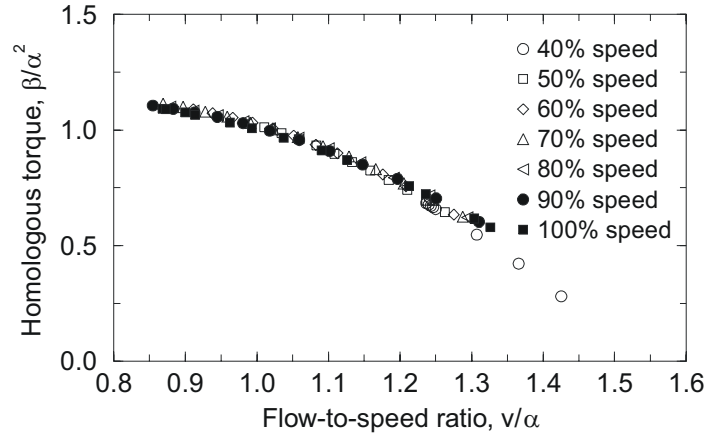


Figure 23. Homologous torque for the recompressing compressor.

Figures 20 through 23 suggest that the homologous curves can be used to extrapolate the effects of a large change in shaft speed, such as occurs during a transient initiated by a loss of external load. However, the large extrapolation required indicates that the results obtained must be considered preliminary.

The shaft speed following a loss of external load is governed by the imbalance of torques on the shaft due to the fluid and the generator. The acceleration of the shaft is significantly affected by the moments of inertia of all the components coupled to the shaft. The moments of inertia for the shaft, turbine, main compressor, and recompressing compressor were calculated or estimated from design data. However, no information was available about the generator. The moment of inertia for the generator was assumed to be $1000 \text{ kg}\cdot\text{m}^2$, which corresponds to about 40% of the total inertia.

The transient initiated by a loss of external load was simulated using the ATHENA model illustrated in Figures 8 through 10 with the compressors replaced by centrifugal pumps as described above. Control and protective systems were assumed to not operate during the transient. Frictional torques due to bearing losses were neglected to maximize the overspeed of the shaft. The transient was initiated by an instantaneous loss of external load, which was assumed to occur at 5.0 s.

The overall behavior of the GFR is illustrated in Figure 24, which shows the response of reactor power, shaft speed, and turbine flow during a transient initiated by a loss of external load. Each parameter was normalized to unity by dividing by its initial value. The loss of external load initially caused a rapid increase in shaft speed that caused the head developed by the compressors to increase as evidenced by the pressures shown in Figure 25. The increase in pump head caused the flow rate through the turbine to increase. The increased flow through the reactor resulted in a slight cooling of the reactor fluid and fuel temperatures as shown in Figure 26. The increase in reactor pressure caused the coolant density to increase, which initially resulted in a small negative reactivity insertion as shown in Figure 27 and a slight decrease in reactor power. Eventually, the reduction in fuel temperature and the resulting positive reactivity insertion due to Doppler feedback and (negative) thermal expansion caused the power to increase slightly. By 20 s, the shaft speed, pressures, and flow rates had stabilized at new values, but the reactor power and temperatures had not yet reached steady values.

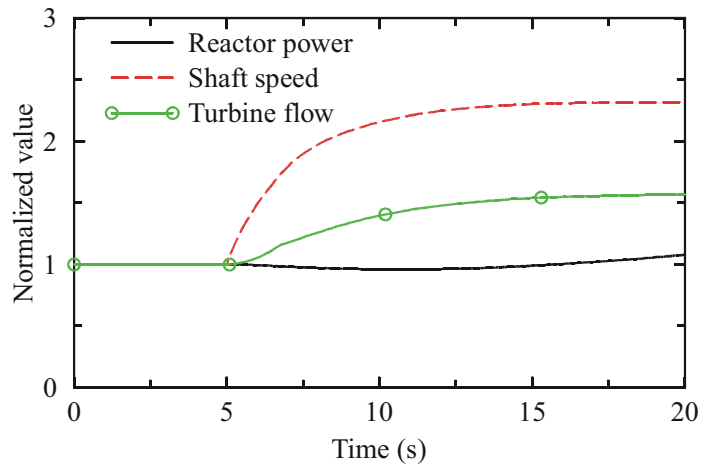


Figure 24. Normalized parameters following a loss of external load.

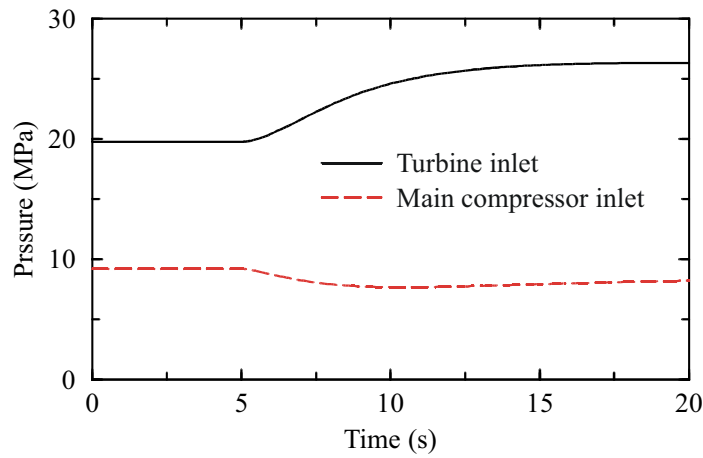


Figure 25. Pressures at the inlet to the turbine and main compressor following a loss of external load.

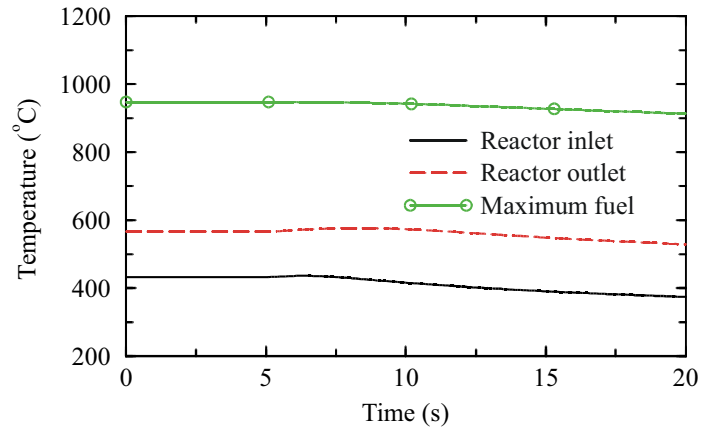


Figure 26. Reactor thermal performance following a loss of external load.

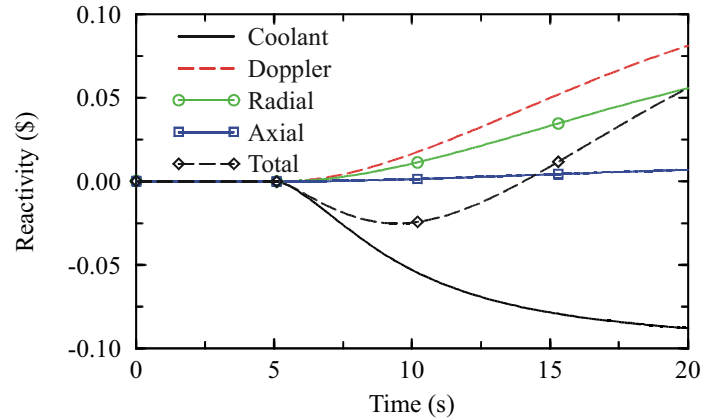


Figure 27. Reactivity feedback following a loss of external load.

Fuel temperature limits are not of concern following a loss of external load because the increased flow through the core causes fuel temperatures to decrease. Reactivity feedback results in only a small increase in reactor power. The principal concern during this transient is the maximum speed of the shaft and its effect on the structural integrity of the turbomachinery. The maximum shaft speed obtained in the ATHENA calculation was more than two times its initial value and is definitely of potential concern. The maximum shaft speed could be reduced by the use of a control system to bypass flow around the turbine. The results presented here are considered preliminary because of the lack of detailed information concerning the moments of inertia of the various components and the lack of compressor performance curves at high shaft speeds.

Heat Transfer Correlation

The maximum, steady-state fuel temperature presented in Table 2 was obtained using the code's default heat transfer package, which simulates forced convection heat transfer using the Dittus-Boelter (1930) heat transfer correlation, in the core. A review (INEEL 2003b) indicates that the Dittus-Boelter correlation agrees well with data for liquids, but predicts values that are about 10% too high for helium gas with small temperature differences between the wall and bulk fluid. To account for large temperature differences, Gnielinski (1976) recommends a correction factor that depends on the ratio of the bulk temperature to the wall temperature. A sensitivity calculation was performed in which the Gnielinski correlation was applied in the core rather than the Dittus-Boelter correlation. The Gnielinski correlation predicted a 20% reduction in the heat transfer coefficient in the core compared to the Dittus-Boelter correlation, with the large temperature difference correction accounting for about half of the reduction. The reduced heat transfer coefficient resulted in a 79 K increase in the maximum fuel temperature at steady state. Because the results obtained with the Gnielinski correlation are expected to be more accurate for the conditions in the GFR, future analyses should be performed using the Gnielinski correlation rather than the Dittus-Boelter correlation.

CONCLUSIONS

Significant improvements have been made to RELAP5/ATHENA for the simulation of the GFR. These improvements include the addition of carbon dioxide as a working fluid, enhancements to

the turbine model, the development of a compressor model, and the addition of the Gnielinski forced convection heat transfer correlation.

A system model of the GFR has been developed for analysis of the transients in which the GFR interacts with the PCU. Comparisons between results of the ATHENA system model and design calculations indicate that the model represents the turbine, compressor, and heat exchanger components reasonably well during steady-state operation.

The analysis of a transient initiated by a reactor trip shows that the GFR responds relatively slowly. The control system does not have to respond rapidly to protect the turbomachinery following a reactor trip. Because the compressors and turbine are connected to a single shaft, the reactor flow remains nearly constant following the trip.

A loss of external load in the GFR results in an increase in flow through the core and thus does not challenge fuel temperature limits. However, the loss of load results in a rapid overspeed of the shaft with the potential to damage the turbomachinery. Assuming no action of the control system, the shaft speed will increase to more than two times its initial value speed within a few seconds of the start of the event. Thus, the control system will have to respond quickly to prevent excessive shaft speed. The absolute values of the calculated results are considered preliminary because of the lack of compressor performance maps at high speeds and detailed design information concerning moments of inertia of the various components connected to the shaft.

The Gnielinski correlation should be used to calculate convective heat transfer from the core in future simulations of the GFR. A sensitivity calculation showed that the maximum, steady-state fuel temperature increased about 80°C when the Gnielinski correlation was used rather than the Dittus-Boelter correlation. A review of the correlations indicated that the Gnielinski correlation should be more accurate than the Dittus-Boelter correlation for the conditions expected in the GFR.

ACKNOWLEDGMENTS

Work supported through the INL Laboratory Directed Research & Development (LDRD) Program under DOE Idaho Operations Office Contract DE AC07 05ID14517.

REFERENCES

Coryell, E. W. and C. B. Davis, 2002, *Implementation of Carbon Dioxide Thermodynamic and Transport Properties into ATHENA*, RELAP5-3D Internal Report R5/3D-02-06, November 2002.

Dittus, F. W. and L. M. K. Boelter, 1930, "Heat Transfer in Automobile Radiators of the Tubular Type," *Publications in Engineering*, 2, University of California, Berkeley, pp. 443-461.

Dostal, V., M. J. Driscoll, P. Hejzlar, and N. E. Todreas, 2002, *CO2 Brayton Cycle Design and Optimization*, MIT-ANP-TR-090, November 2002.

Dostal, V., M. J. Driscoll, and P. Hejzlar, 2004, *A Supercritical Carbon Dioxide Cycle for Next Generation Nuclear Reactors*, MIT-ANP-TR-100, March 10, 2004.

2005 RELAP5 International Users Seminar
Jackson Hole, Wyoming
September 7-9, 2005

J. E. Fisher and C. B. Davis, 2005, "RELAP5-3D Compressor Model," *Space Nuclear Conference, ANS Meeting, San Diego, CA, June 5-9, 2005*.

Gnielinski, V., 1976, "New equations for heat and mass transfer in turbulent pipe and channel flow," *International Chemical Engineering*, Vol. 16, No. 2, 359-368.

Hejzlar, P., 2004a, Personal communication with C. B. Davis, February 6, 2004.

Hejzlar, P., 2004b, Personal communication with C. B. Davis, April 16, 2004.

Hejzlar, P., 2004c, Personal communication with C. B. Davis, July 19, 2004.

INEEL, 2003a, *RELAP5-3D Code Manual, Code Structure, System Models, and Solution Methods, Vol. 1*, INEEL-EXT-98-00834, Revision 2.2, October 2003.

INEEL, 2003b, *RELAP5-3D Code Manual, Models and Correlations, Vol. 4*, INEEL-EXT-98-00834, Revision 2.2, October 2003.

Lemmon, E. W., M. O. McLinden, and M. L. Huber, 2002, *REFPROP Reference Fluid Thermodynamic and Transport Properties, NIST Standard Reference Database 23, Version 7.0 Beta Version*, National Institute of Standards and Technology, 2002.

MacDonald, P. E. and J. Buongiorno, *Design of an Actinide Burning, Lead or Lead-Bismuth Cooled Reactor That Produces Low Cost Electricity*, FY-01 Annual Report, INEL/EXT-01-01376, MIT-ANP-PR-083, October 2001.

MacDonald, P. E., J. W. Sterbentz, R. L. Sant, P. D. Bayless, R. R. Schultz, H. D. Gougar, R. L. Moore, A. M. Ougououag, and W. K. Terry, 2003, *NGNP Preliminary Point Design – Results of the Initial Neutronics and Thermal-Hydraulic Assessments*, Revision 1, INEEL/EXT-03-00870, September 2003.

Marshall, T., K. Weaver, and C. Davis, 2005, "Implications of Passive Decay Heat Removal During a LOCA with a Gas-cooled Gas Reactor," Paper 5708, *Proceedings of ICAPP '05, Seoul, Korea May 15-19, 2005*.

McLinden, M. O. et al., 1998, *NIST Thermodynamic and Transport Properties of Refrigerants and Refrigerant Mixtures — REFPROP, Version 6.01 Users' Guide*, U. S. Department of Commerce, NIST Standard Reference Database 23, July 1998.

Perry, J. H., *Chemical Engineers' Handbook*, Third Edition, McGraw-Hill Book Company, 1950.

Vesovic, V. et al, "The Transport Properties of Carbon Dioxide," *J. Phys. Chem. Ref. Data*, Vol. 19, No. 3, 1990.

Wang, Y., 2003, *Aerodynamic Design of Turbine for S-CO₂ Brayton Cycle*, MIT-GFR-003, June 2003.